

Mode Recognition by Shape Morphing for Maxwell's Eigenvalue Problem

Anna Ziegler, Niklas Georg, Wolfgang Ackermann, Sebastian Schöps

Abstract—In electrical engineering, for example during the design of superconducting radio-frequency cavities, eigenmodes must be identified based on their field patterns. This allows to understand the working principle, optimize the performance of a device and distinguish desired from parasitic modes. For cavities with simple shapes, the eigenmodes are easily classified according to the number of nodes and antinodes in each direction as is obvious from analytical formulae. For cavities with complicated shapes, the eigenmodes are determined numerically. Thereby, the classification is cumbersome, if not impossible. In this paper, we propose a new recognition method by morphing the cavity geometry to a pillbox and tracking its eigenmodes during the deformation.

Index Terms—Electromagnetic Wave Equation, Resonant Cavities, Eigenmodes, Isogeometric Analysis

I. INTRODUCTION

CAVITY resonators are structures in which a standing wave, with different modes and frequencies, is formed by resonance. One of the most well-known examples of a lossless resonator is the pillbox cavity, see Fig. 1a. Modern resonators have more complex shapes, e.g. each cell of the superconducting radiofrequency TESLA cavity [1] that is used for particle acceleration has been constructed by several ellipses quantified in terms of six geometry parameters (lengths and radii), see Fig. 1b. Since the shape is a major design choice, computer simulation, shape optimization and uncertainty quantification are part of nowadays design processes [2], [3], [4].

Originally, low order discretization methods, e.g. based on the finite difference or finite integration method, were used to numerically approximate the underlying Maxwell eigenvalue problem, see e.g. [5], [6], [7]. Nowadays, finite elements (FE) with higher-order basis functions and curved elements are state of the art [8], [9]. Recently, a new finite-element variant called isogeometric analysis (IGA) was proposed by Cottrell et al. [10] and firstly applied to the simulation of cavities, by

Manuscript received xxxx yy, 2022; revised xxxxx y, 2022; accepted xxxxx y, 2022. Date of publication xxxxx y, 2022; date of current version xxxxx y, 2022. All authors are with the institute for Accelerator Science and Electromagnetic Fields (TEMF) at TU Darmstadt, Darmstadt, Germany (e-mails: anna.ziegler@tu-darmstadt.de, wolfgang.ackermann@tu-darmstadt.de, sebastian.schoeps@tu-darmstadt.de). A. Ziegler, N. Georg and S. Schöps are with the Graduate School of Computational Engineering at TU Darmstadt, Darmstadt, Germany. The authors thank Herbert De Gerssem, Jacopo Corno and Mario Mally for the support and the many fruitful discussions. This work is supported by the Graduate School CE within the Centre for Computational Engineering at Technische Universität Darmstadt and by the Federal Ministry of Education and Research (BMBF) and the state of Hesse as part of the NHR Program. Corresponding author: A. Ziegler. Color versions of one or more of the figures in this article are available online at <http://ieeexplore.ieee.org>. Digital Object Identifier 10.1109/TAP.2022.xxxxxxx

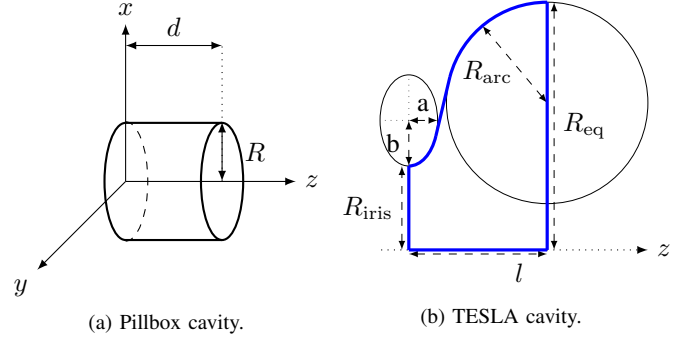


Fig. 1. Geometrical shape of pillbox and TESLA cavity.

Corno et al. [11]. IGA uses the same spline-based functions from computer-aided-design (CAD) to describe solution and geometry such that no geometry-related modeling error is introduced. This is particularly useful when dealing with problems that are sensitive with respect to their geometric shape.

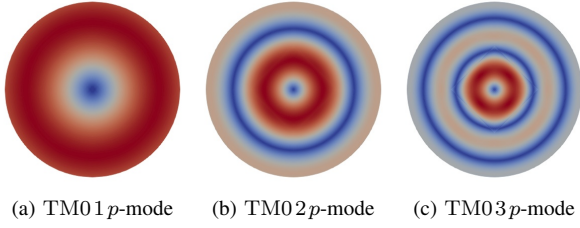
In accelerator science, often many eigenmodes and eigenfrequencies must be computed by solving Maxwell's eigenvalue problem, for example Ackermann et al. and Wanzenberg investigate the first 194 modes and 196 modes, respectively, of the TESLA cavity for DESY in [12], [13]. They identify the modes and the corresponding passbands entirely manually or based on the azimuthal classification since a reliable automatic mode recognition is not available until today. Existing approaches may identify modes wrongly or are not applicable in the case of multiple cells or high frequencies, see [14]. To this end, we propose here a new method that is based on shape morphing and eigenvalue tracking: we gradually deform the geometry of a complex shaped cavity to a simple one, e.g., the cylindrical pillbox. This allows us to uniquely identify each eigenpair of the complex shaped cavity with one of the pillbox, where modes, frequencies and their categorization are known in closed form, e.g.,

$$\omega_{\text{TM},mnp} = \frac{1}{\sqrt{\mu\epsilon}} \sqrt{\frac{x_{mn}^2}{R^2} + \frac{p^2\pi^2}{d^2}} \quad (1)$$

resp.

$$\omega_{\text{TE},mnp} = \frac{1}{\sqrt{\mu\epsilon}} \sqrt{\frac{x'_{mn}}{R^2} + \frac{p^2\pi^2}{d^2}}, \quad (2)$$

where μ denotes the permeability, ϵ the permittivity, R indicates the radius and d the length of the pillbox. The expression x_{mn} indicates the n th root of the Bessel function $J_m(x) = 0$ and x'_{mn} the n th root of $J'_m(x) = 0$. Integers m, n



(a) TM01 p -mode (b) TM02 p -mode (c) TM03 p -mode

Fig. 2. Exemplary mode patterns in pillbox cavity, where p is an arbitrary integer value denoting the number of half-waves in longitudinal direction (not identifiable in 2D).

and p take on the values $m = 0, 1, 2, \dots$, $n = 1, 2, 3, \dots$ and $p = 0, 1, 2, \dots$, where the lowest transverse magnetic (TM) mode has $m = p = 0$ and $n = 1$ (hence is classified as TM010). The lowest transverse electric (TE) mode has $m = n = p = 1$ (hence TE111). Details can be found in [15, Section 8.7] and the patterns of the first three TM modes are visualized in Fig. 2.

The paper is structured as follows. In Section II we describe the geometry and the parametrization of the computational domain. Subsequently, we state the Maxwell eigenvalue problem and introduce its isogeometric discretization in Section III. In Section IV we present our mode classification algorithm and the possibility to use it both for identifying and for exploring modes in a complex cavity geometry. We demonstrate the application of our algorithm for conveying the well-known mode nomenclature of the cylindrical pillbox cavity to more complex cavities in Section V. Furthermore, we automatically recognize modes of the TESLA cavity by morphing its shape to the pillbox cavity and discuss the results. We conclude our work in Section VI.

II. DOMAIN PARAMETRIZATION

Due to the relevance of the cavity shape, we start with a brief summary of geometry description in terms of CAD [16]. The physical domain Ω is represented as a mapping

$$\mathbf{G} : \hat{\Omega} \rightarrow \Omega \quad (3)$$

from a reference domain $\hat{\Omega}$. In CAD, this reference domain is commonly the unit cube $\hat{\Omega} = [0, 1]^3$. If a shape is too complex to be represented by a single mapping, one uses several mappings, also called patches, to represent the overall geometry. Each patch is given by a B-spline or Non-Uniform Rational B-spline (NURBS) curve. We discuss here, for simplicity, only the case of a trivariate B-spline mapping, i.e.,

$$\mathbf{G}(\hat{\mathbf{x}}) = \sum_{i=1}^{n_1} \sum_{j=1}^{n_2} \sum_{k=1}^{n_3} \mathbf{P}_{i,j,k} B_{i,p_1} B_{j,p_2} B_{k,p_3} \quad (4)$$

with control points $\mathbf{P}_{i,j,k}$ that form the so-called control mesh. The case of NURBS is similar but requires the introduction of an additional weighting. Each B-spline basis functions $\{B_{i,p}\}_{i=1}^N$ stems from a one-dimensional B-spline space S_α^p of degree p and regularity α [16, Chapter 7]. They are

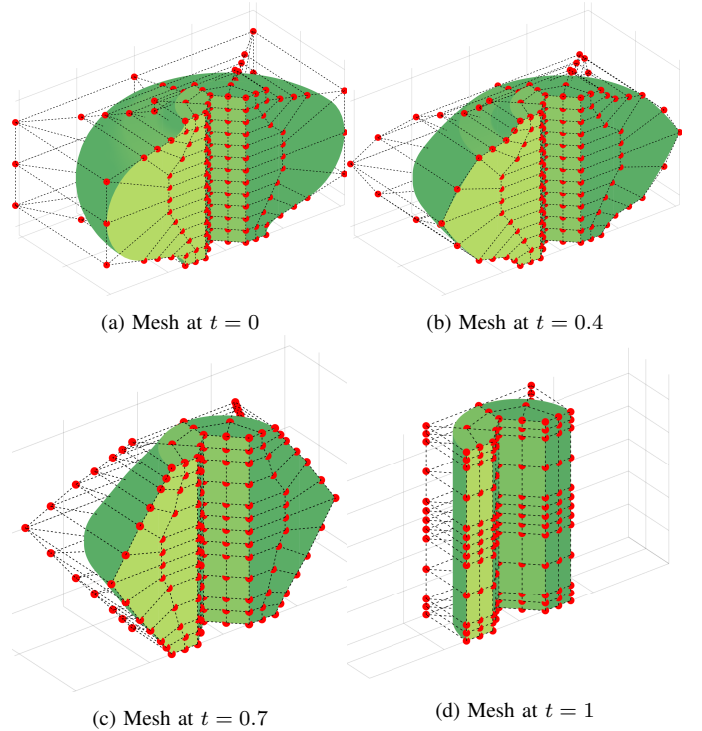


Fig. 3. Illustration of a mesh deformation which transforms the shape of a TESLA cell to a pillbox shape. The control points are illustrated in red. The full cavity is composed of 5 patches, see [18, Section 3.6] for details.

constructed from a knot vector $\Xi = (\xi_1, \xi_2, \dots, \xi_n) \in [0, 1]^n$, $\xi_1 \leq \xi_2 \leq \dots \leq \xi_n$ using the Cox-de Boor algorithm [17]

$$B_{i,0}(\xi) = \begin{cases} 1 & \text{if } \xi_i \leq \xi < \xi_{i+1} \\ 0 & \text{otherwise} \end{cases}$$

$$B_{i,p}(\xi) = \frac{\xi - \xi_i}{\xi_{i+p} - \xi_i} B_{i,p-1}(\xi) + \frac{\xi_{i+p+1} - \xi}{\xi_{i+p+1} - \xi_{i+1}} B_{i+1,p-1}(\xi).$$

Varying the control points allows us to gradually morph one shape to another. For this paper it is sufficient to consider linear transformations of the control points: let us assume we have two cavities represented by two mappings $\mathbf{G}^{(1)}$ and $\mathbf{G}^{(2)}$ with matching control meshes, i.e. $\mathbf{P}_{i,j,k}^{(1)}$ and $\mathbf{P}_{i,j,k}^{(2)}$ of compatible dimensions. Then, we morph one into the other by the convex combination

$$\mathbf{P}_{i,j,k}(t) := (1-t)\mathbf{P}_{i,j,k}^{(1)} + t\mathbf{P}_{i,j,k}^{(2)}$$

when varying $t \in [0, 1]$, see Fig. 3. This gives rise to a parametrized version of (4)

$$\mathbf{G}_t(\hat{\mathbf{x}}) = \sum_{i=1}^{n_1} \sum_{j=1}^{n_2} \sum_{k=1}^{n_3} \mathbf{P}_{i,j,k}(t) B_{i,p_1} B_{j,p_2} B_{k,p_3} \quad (5)$$

and as a result also to the parametrized computational domain Ω_t .

III. PROBLEM STATEMENT

Let us formulate in this section the electromagnetic field problem and its discretization.

A. Maxwell's Eigenvalue Problem

Starting from Maxwell's equations on the domain Ω_t , with homogeneous, lossless materials, perfect electric boundary conditions on $\partial\Omega_t$ and without sources, one derives Maxwell's eigenvalue problem: find wave numbers $k := \omega\sqrt{\mu\varepsilon} \in \mathbb{R}^+$ and $\mathbf{E} \neq 0$ such that

$$\begin{aligned} \operatorname{curl}(\operatorname{curl} \mathbf{E}) &= k^2 \mathbf{E} && \text{in } \Omega_t \\ \mathbf{E} \times \mathbf{n} &= 0 && \text{on } \partial\Omega_t. \end{aligned} \quad (6)$$

The weak formulation is obtained by testing and integration. The resulting problem reads: find $k \in \mathbb{R}^+$ and $\mathbf{E} \in H_0(\operatorname{curl}; \Omega_t)$ such that

$$(\operatorname{curl} \mathbf{E}, \operatorname{curl} \mathbf{v}) = k^2 (\mathbf{E}, \mathbf{v}) \quad \forall \mathbf{v} \in H_0(\operatorname{curl}; \Omega_t), \quad (7)$$

where we made use of the function space of square-integrable vector fields with square-integrable curl and vanishing trace $H_0(\operatorname{curl}; \Omega_t)$, see [19]. Following the Ritz-Galerkin paradigm, we represent the unknown solution by basis functions \mathbf{v}_j from the same space, i.e.,

$$\mathbf{E} = \sum_j e_j \mathbf{v}_j. \quad (8)$$

Finally, we approximate the solution by considering only a finite-dimensional subspace $V_h \subset H_0(\operatorname{curl}; \Omega_t)$ of dimension $N = \dim V_h$. We obtain the generalized eigenvalue problem: find all \mathbf{e} and λ such that

$$\mathbf{K}\mathbf{e} = \lambda \mathbf{M}\mathbf{e}, \quad (9)$$

where $\lambda = k^2$, the parameter-dependent stiffness and mass matrices are expressed by

$$\begin{aligned} \mathbf{K}_{i,j}(t) &= \int_{\Omega_t} \operatorname{curl} \mathbf{v}_j \cdot \operatorname{curl} \mathbf{v}_i \, dx, \\ \mathbf{M}_{i,j}(t) &= \int_{\Omega_t} \mathbf{v}_j \cdot \mathbf{v}_i \, dx \end{aligned} \quad (10)$$

with $i, j = 1, \dots, N$. The parameter-dependence of the matrices is naturally inherited by the solutions of the eigenvalue problem

$$\lambda = \lambda(t), \quad \text{and} \quad \mathbf{e} = \mathbf{e}(t) \quad (11)$$

depending on the parameter t . Georg et al. [3] propose algebraic, simplified matrix mappings to replace (10), i.e.

$$\tilde{\mathbf{K}}(t) := (1-t)\mathbf{K}(0) + t\mathbf{K}(1) \quad (12a)$$

$$\tilde{\mathbf{M}}(t) := (1-t)\mathbf{M}(0) + t\mathbf{M}(1). \quad (12b)$$

They also allow to match eigenvalues from $t = 0$ to $t = 1$. The construction in (12) exploits the fact that the discretizations of $\Omega^{(1)}$ and $\Omega^{(2)}$ and thus also the matrix dimensions are compatible. The advantage is that the matrix-valued functions $\tilde{\mathbf{K}}(t)$ and $\tilde{\mathbf{M}}(t)$ are linear in t , while $\mathbf{K}(t)$ and $\mathbf{M}(t)$ have a nonlinear dependence. This will reduce numerical costs for matrix assembly and makes derivative computations, e.g. $d/dt \tilde{\mathbf{M}}(t)$, trivial. However, the original functions (10) always correspond to *physical* geometries, while (12) are purely *algebraic* and have no geometric counterpart for $0 < t < 1$.

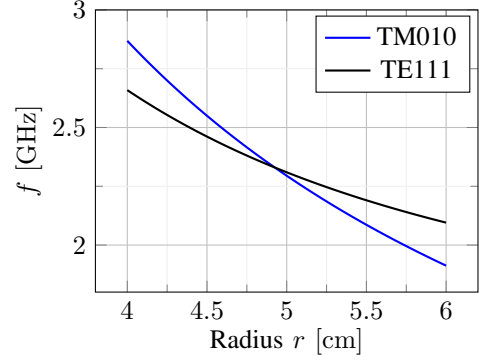


Fig. 4. Crossing of eigenvalues of TM010 and TE111 at $r = 4.92$ cm demonstrated for pillbox cavity.

B. Basis Functions

The various FE methods differ in the construction of the approximation space V_h , e.g. basis functions of different order, element types etc. We refer to [19], [20] for the classical FE method. However, we will follow [21] and employ IGA using curl-conforming B-splines. This allows us to use the same basis functions for the discretization as for the geometry description, i.e., without an additional meshing step.

The B-spline space of degree p_i along dimension i , with regularity C^{α_i} , on the domain $\hat{\Omega}$ shall be denoted by $S_{\alpha_1, \alpha_2, \alpha_3}^{p_1, p_2, p_3}(\hat{\Omega})$. Then, following [21], the discrete space \hat{V}_h is chosen as

$$\hat{V}_h := S_{\alpha_1-1, \alpha_2, \alpha_3}^{p_1-1, p_2, p_3} \times S_{\alpha_1, \alpha_2-1, \alpha_3}^{p_1, p_2-1, p_3} \times S_{\alpha_1, \alpha_2, \alpha_3-1}^{p_1, p_2, p_3-1}. \quad (13)$$

Finally, the discrete space V_h in the physical domain is obtained through a curl-conforming transformation [19] using our domain transformation G_t from (5). In [21] it is shown that the B-spline basis functions from these spaces form a discrete de Rham sequence in both, the reference and physical domain, such that they are suitable for the discretization of $H(\operatorname{curl}; \Omega)$. We employ the open source implementation GeopDEs in Matlab for the discretization [22], [23].

IV. SHAPE MORPHING

To classify eigenmodes, we propose to follow the eigenvalues and eigenvectors along $t \in T = [0, 1]$ from the complex geometry to a simple geometry, e.g. pillbox. This allows to use the established nomenclature from field theory [15, Section 8.7] and is less error-prone than methods based on counting zero-crossing or maxima [14] as we will demonstrate in Section V. However, our classification method requires a numerical tracking procedure of the eigenpairs [24], [25], [26], [3]. This is necessary since eigenvalues may cross on T , see Fig. 4, such that a numbering with respect to the magnitude of the eigenvalues at a given t is not reliable.

A. Eigenvalue Tracking

We discretize the parameter interval T into $0 = t_1 < t_2 < \dots < t_i < \dots < t_M = 1$. Then we compute sequentially for each i the relevant eigenpairs $j \in J \subset \{1, \dots, N\}$ by solving (9) on geometry Ω_{t_i} . Let us assume we have solved

the eigenvalue problem (9) at step i by an eigenvalue solver, e.g. an Arnoldi or Lanczos method [27]. The solutions are denoted by $\mathbf{e}_{i,j} := \mathbf{e}_j(t_i)$ and $\lambda_{i,j} := \lambda_j(t_i)$. We now aim at computing the eigenpairs for step $i+1$ but since an eigenvalue crossing may occur between t_i and t_{i+1} , the consistent sorting of the eigenpairs at t_{i+1} must be determined. We denote the unsorted candidates from solving the eigenvalue problem (9) on $\Omega_{t_{i+1}}$ by $\hat{\mathbf{e}}_{i+1,k}$ and $\hat{\lambda}_{i+1,k}$. They are compared with first-order extrapolations from the current step, i.e.,

$$\begin{bmatrix} \tilde{\mathbf{e}}_{i+1,j} \\ \tilde{\lambda}_{i+1,j} \end{bmatrix} = \begin{bmatrix} \mathbf{e}_{i+1} \\ \lambda_{i+1} \end{bmatrix} + h_i \begin{bmatrix} \mathbf{e}'_{i,j} \\ \lambda'_{i,j} \end{bmatrix} \quad (14)$$

to establish the matching where we used $h_i := t_{i+1} - t_i$ for the stepsize. In the case of non-degenerated eigenpairs the derivatives are easily obtained by solving

$$\begin{bmatrix} \mathbf{K}_i - \lambda_{i,j} \mathbf{M}_i & -\mathbf{M}_i \mathbf{e}_{i,j} \\ \mathbf{e}_{i-1,j}^H \mathbf{M}_i & 0 \end{bmatrix} \begin{bmatrix} \mathbf{e}'_{i,j} \\ \lambda'_{i,j} \end{bmatrix} = \begin{bmatrix} -\mathbf{K}'_i \mathbf{e}_{i,j} + \lambda_{i,j} \mathbf{M}'_i \mathbf{e}_{i,j} \\ -\mathbf{e}_{i-1,j}^H \mathbf{M}'_i \mathbf{e}_{i,j} \end{bmatrix} \quad (15)$$

where we used the definitions $\mathbf{K}_i := \mathbf{K}(t_i)$, $\mathbf{M}_i := \mathbf{M}(t_i)$ and added a normalization constraint based on $\mathbf{e}_{i-1,j}$. Finally, we use the correlation factor proposed by [25]

$$\varphi_{i+1,k,j} = \frac{\hat{\mathbf{e}}_{i+1,k}^H \mathbf{M}_{i+1} \tilde{\mathbf{e}}_{i+1,j}}{\|\hat{\mathbf{e}}_{i+1,k}\|_{\mathbf{M}_{i+1}} \|\tilde{\mathbf{e}}_{i+1,j}\|_{\mathbf{M}_{i+1}}} \quad (16)$$

with the norm $\|\mathbf{x}\|_{\mathbf{A}} = \sqrt{\mathbf{x}^H \mathbf{A} \mathbf{x}}$ for the matching. The correlation factor compares the normalized scalar products of the predicted eigenvectors $\tilde{\mathbf{e}}_{i+1,j}$ and the new candidates $\hat{\mathbf{e}}_{i+1,k}$ that are obtained by solving the eigenvalue problem at t_{i+1} . In the ideal case, i.e., the eigenpairs depend linearly on t , we find j and k such that $\hat{\mathbf{e}}_{i+1,k} = \tilde{\mathbf{e}}_{i+1,j}$. Then, the correlation factor is $\varphi_{i+1,k,j} = 1$ and $\varphi_{i+1,l,j} = 0$ for all other $l \neq k$ since it is a product of orthonormal vectors. In the general case, all $\varphi_{i+1,k,j}$ will attain values between 0 and 1 and a correlation is computed for all pairs j, k . We match the one with the highest correlation factor and define

$$\begin{bmatrix} \mathbf{e}_{i+1,j} \\ \lambda_{i+1,j} \end{bmatrix} := \begin{bmatrix} \hat{\mathbf{e}}_{i+1,k} \\ \hat{\lambda}_{i+1,k} \end{bmatrix} \text{ with } \arg \max_{j,k} \{\varphi_{i+1,k,j}\}. \quad (17)$$

To reduce the risk that an eigenpair is wrongly matched, e.g. due to an insufficiently small step size, the new eigenpair is only accepted if it fulfills the criterion

$$\max_{j,k} \varphi_{i+1,k,j} \geq \varphi_{\min}$$

with respect to a user-specified threshold correlation factor φ_{\min} . If the criterion is not met, the step is repeated with a smaller stepsize. The tracking algorithm is illustrated by the flowchart in Fig. 5.

Note that the presented version of the algorithm requires non-degenerated eigenmodes at each t_i . However, the algorithm can be generalized by using Ojalvo's method for computing the derivatives instead of (15), [28], [29]. However, this was not necessary in our computations.

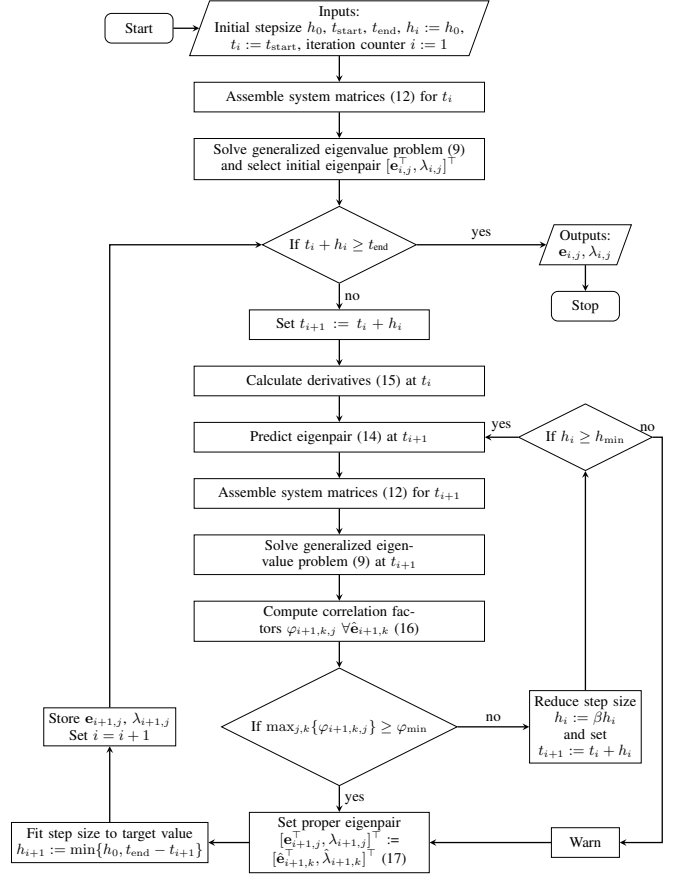


Fig. 5. Flowchart describing the proposed eigenvalue tracking method. The parameter of the stepsize control is chosen as $\beta = 0.5$.

B. Identification of Eigenmodes

We use the eigenvalue tracking as proposed in section IV-A to recognize eigenmodes by tracking the eigenvalues from the complex geometry $\Omega^{(1)}$ without known classification to a geometry $\Omega^{(2)}$ where the eigenmodes, eigenfrequencies and classifications are known, e.g. the pillbox cavity. After having solved the eigenvalue problem (9) at $t = 0$, we choose an eigenpair j for which we want to convey the classification system. We apply the presented algorithm and track the eigenmodes to the geometry $\Omega^{(2)}$ and finally match the result with known closed-form eigenfrequencies, see e.g. (1-2). We can use either the physical (10) or algebraic mapping (12). Both yield the same results as will be demonstrated later in Section V.

C. Exploration of Eigenmodes

The same tracking algorithm can also be used ‘backwards’, i.e. from $t = 1$ down to $t = 0$, to explore a specific eigenmode m, n, p in the complex geometry $\Omega^{(1)}$ for which the number k of the eigenmode \mathbf{e}_k is not known. To specify the eigenmode that should be detected, the known eigenfrequency and corresponding classification are chosen and matched with the numerical solution of the eigenvalue problem (9) on $\Omega^{(2)}$. The eigenmode $\mathbf{e}_{1,j}$ with m, n, p on $\Omega^{(2)}$ is then tracked to the geometry $\Omega^{(1)}$, in which it is to be analyzed.

This procedure allows to compute a single eigenmode in an efficient way. Otherwise possibly many eigenpairs in the assumed vicinity of the desired eigenmode for the geometry $\Omega^{(1)}$ have to be computed and then forwardly tracked until the desired one is identified on $\Omega^{(2)}$.

V. APPLICATION

In this section, we present the application of the identification and exploration to the TESLA cavity and the cylindrical pillbox cavity. The classifications of the eigenmodes of the pillbox cavity into TE and TM modes and according to the field distribution in azimuthal, radial and longitudinal direction are known analytically and are given in (1) and (2).

Following the theory of electromagnetic fields, the azimuthal index m can be related to the number of zero crossings resp. of local field extrema in azimuthal direction and indicates the number of poles of the mode according to a classical multipole expansion, where $m = 0$ refers to a monopole mode, $m = 1$ to a dipole mode, $m = 2$ to a quadrupole mode and so forth. The radial index n corresponds to the number of half-waves in radial direction and the longitudinal index p analogously in longitudinal direction.

The goal is to convey this nomenclature to the TESLA cavity without relying on error-prone counting of zero-crossings or maxima and minima. In order to perform this eigenmode classification automatically, the eigenmodes of the TESLA cavity are tracked along the deformation to the pillbox cavity and matched with the analytical solutions.

A. TESLA Cavity

The TESLA cavity is a radio-frequency superconducting cavity designed for linear accelerators. We use here the design that is installed at DESY in Hamburg, [30]. It is a 9-cell standing wave structure of about 1 m in length, whose accelerating eigenmode resonates at 1.3 GHz. Following [18], instead of the 141.6 mm beampipes with connected higher-order mode (HOM) couplers, cylindrical beampipes with an increased length of 365 mm are attached to the model, such that the effects of the boundary conditions at the end caps of the beampipes on the eigenmodes can be neglected. This approximation is valid for eigenmodes below the cutoff frequency of approximately 2.2 GHz, this includes the first monopole and the first two dipole passbands.

In order to achieve the desired field flatness within the cavity, we conduct a tuning procedure before tracking the eigenmodes, following [18]. We employ two criteria to quantify the field flatness and combine them to a weighted objective function. We denote the peak value of the longitudinal component of the electric field at radius $r = 0$ by $E_{\text{peak},q}$ in the q th cell. To improve the field flatness, we modify the length of the two end-cups of the TESLA cavity and the radius of the cell-equator using a particle swarm optimizer until we reach field flatness with

$$\eta_1 = 1 - \frac{(\max_q |E_{\text{peak},q}| - \min_q |E_{\text{peak},q}|)}{\mathbb{E}(|E_{\text{peak},q}|)} \quad (18)$$

and

$$\eta_2 = 1 - \frac{\text{std}(E_{\text{peak},q})}{\mathbb{E}(|E_{\text{peak},q}|)} \quad (19)$$

TABLE I
PARAMETERS OF THE TESLA HALF-CELLS AND TUNING, ALL DIMENSIONS IN mm [1] AND THE DIFFERENCE DUE TO TUNING, CF. FIG. 1B

cavity shape parameter	midcup (+tuning)	endcup 1 (+tuning)	endcup 2 (+tuning)
equator radius R_{eq}	103.3 (+ 0.89)	103.3	103.3
iris radius R_{iris}	35	39	39
radius R_{arc} of arc	42.0	40.3	42
horizontal half axis a	12	10	9
vertical half axis b	19	13.5	12.8
length l	57.7	56.0 (+0.90)	57.0 (+1.04)

of $\eta_1, \eta_2 \geq 0.95$. The parameters for the construction of the TESLA cavity and our tuning values are shown in Tab. I. With those tuning values, we achieve a field flatness with $\eta_1 = 0.9907$ and $\eta_2 = 0.9965$.

Solving (15) requires the derivatives \mathbf{K}'_i and \mathbf{M}'_i . While the computation of the derivatives for the algebraic matrix mappings (12) is trivial due to their linear construction, we compute the derivatives for the geometric matrices (10) by finite differences

$$\mathbf{K}'(t) := \frac{d}{dt}\mathbf{K}(t) \approx \frac{1}{\delta}(\mathbf{K}(t+\delta) - \mathbf{K}(t)) \quad (20a)$$

$$\mathbf{M}'(t) := \frac{d}{dt}\mathbf{M}(t) \approx \frac{1}{\delta}(\mathbf{M}(t+\delta) - \mathbf{M}(t)), \quad (20b)$$

with sufficiently small δ .

We start our algorithm with an initial stepsize of $h_0 = 0.1$ and decrease the stepsize by $\beta = 0.5$ if the maximum correlation factor is smaller than $\varphi_{\text{min}} = 0.9$. If the stepsize h_i gets smaller than e.g. $h_{\text{min}} = 0.00125$, we accept the current eigenpair nevertheless and issue a warning. For the computation of the finite differences, we use $\delta = 10^{-6}$.

B. Shape morphing

In order to classify the eigenmodes of the TESLA cavity by applying the eigenvalue tracking as described in section IV-A, we consider a linear shape morphing from the 9-cell TESLA cavity to a pillbox cavity of radius $r = 3.9$ cm and length $l = 103.61$ cm (+0.19 cm). This corresponds to the iris radius of the TESLA cavity endcaps and the length of the (tuned) TESLA cavity without the beampipes, respectively, see Tab. I. The CAD data are given for download in [31]. The model of the cavity is discretized using second degree basis functions and 24 960 degrees of freedom. The morphing of the shape of the 9-cell TESLA cavity (using the physical mapping) and the concomitant deformation of the magnitude of the electric field within the cavity is illustrated in Fig. 6 from the original TESLA cavity at deformation parameter $t = 0$ in Fig. 6a to the pillbox cavity at $t = 1$ in Fig. 6f for the accelerating eigenmode TM018.

C. Identification of Eigenmodes

The eigenmode tracking algorithm is applied to the first 45 eigenmodes of the TESLA cavity, corresponding to the first monopole passband and the first and second dipole passband. The results are presented in Table II, ordered by the eigenfrequency.

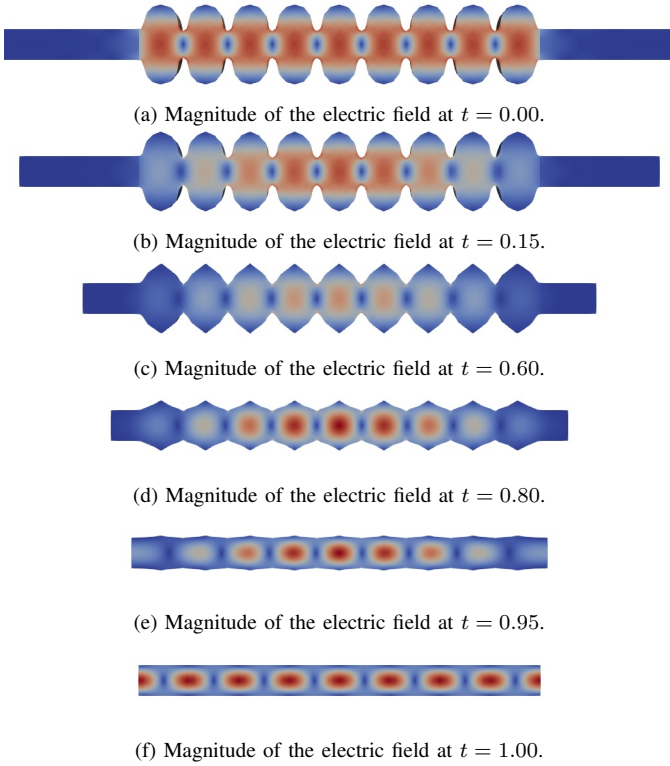


Fig. 6. Electric field magnitude of the accelerating eigenmode (TM018) along the physical deformation.

As one can see, the first nine eigenmodes are monopole modes with radial index $n = 1$ and longitudinal index p from 0 to 8. The accelerating eigenmode is the 9th eigenmode, which is classified as TM018, for which the magnitude of the electric field can be seen in Fig. 6. These and further visualizations are accessible in [31]. The next 18 eigenmodes correspond to the first dipole mode passband, where each eigenmode appears twice, with different polarisation. Eigenmodes $j = 28, \dots, 45$ belong to the second dipole passband with longitudinal index p from 10 to 18. We note that our classification of the second dipole passband differs from the established nomenclature, as e.g. in [13]. However, this is not surprising since the longitudinal components of the corresponding modes in the TESLA cavity do not allow an unambiguous assignment of TE or TM since both \mathbf{E}_z and \mathbf{H}_z components are not identically zero.

The tracking plot for the first monopole passband (modes $j = 1, \dots, 9$) can be seen in Fig. 7 for both mappings, indicated in different colors. We can observe that both the algebraic and the physical mapping yield the same classification in the pillbox cavity.

Fig. 8 visualizes the tracking results for the first 45 eigenmodes in the TESLA cavity. We can see that the tracking yields smooth results. The crossings of the eigenvalues and the overlapping of eigenmode passbands emphasize the need for a tracking procedure to clearly match and classify the eigenmodes along the shape morphing.

Our eigenmode classification method is not limited to the

TABLE II
IDENTIFICATION RESULTS FOR THE FIRST 45 EIGENMODES OF THE TESLA CAVITY. THE DIFFERENT PASSBANDS ARE SEPARATED BY HORIZONTAL LINES.

type	m	n	p	Mode	Freq. (GHz) [12]	Freq. (GHz)	Rel. Error ($\cdot 10^{-4}$)
TM	0	1	0	1	1.2763	1.2759	3.301168
TM	0	1	1	2	1.2784	1.278	3.347528
TM	0	1	2	3	1.2816	1.2812	3.166773
TM	0	1	3	4	1.2855	1.2852	2.554033
TM	0	1	4	5	1.2898	1.2894	2.825461
TM	0	1	5	6	1.2938	1.2935	2.532468
TM	0	1	6	7	1.2971	1.2968	2.426407
TM	0	1	7	8	1.2993	1.299	2.626834
TM	0	1	8	9	1.3	1.2997	2.091273
TE	1	1	1	10	1.6205	1.6235	18.464258
TE	1	1	2	11	1.6206	1.6235	17.846063
TE	1	1	3	12	1.628	1.6306	15.824672
TE	1	1	4	13	1.6282	1.6306	14.594378
TE	1	1	5	14	1.6408	1.6429	12.562058
TE	1	1	6	15	1.641	1.6429	11.341758
TE	1	1	7	16	1.6585	1.6603	10.599798
TE	1	1	8	17	1.6587	1.6603	9.392756
TE	1	1	9	18	1.6806	1.6822	9.484479
TE	1	1	10	19	1.6809	1.6822	7.698028
TE	1	1	11	20	1.7061	1.7077	9.374655
TE	1	1	12	21	1.7063	1.7077	8.20143
TE	1	1	13	22	1.7335	1.7355	11.417331
TE	1	1	14	23	1.7338	1.7355	9.685052
TE	1	1	15	24	1.7614	1.764	14.857441
TE	1	1	16	25	1.7616	1.764	13.720423
TE	1	1	17	26	1.7886	1.7923	20.439801
TE	1	1	18	27	1.789	1.7923	18.199345
TE	1	1	19	28	1.7992	1.8064	39.785396
TE	1	1	20	29	1.7995	1.8064	38.111634
TE	1	1	21	30	1.8375	1.8396	11.419085
TE	1	1	22	31	1.8375	1.8396	11.419085
TE	1	1	23	32	1.8531	1.857	20.880189
TE	1	1	24	33	1.8532	1.857	20.339455
TE	1	1	25	34	1.8655	1.8706	27.084683
TE	1	1	26	35	1.8655	1.8706	27.084683
TE	1	1	27	36	1.8746	1.8806	31.825022
TE	1	1	28	37	1.8746	1.8806	31.825022
TE	1	1	29	38	1.8809	1.8876	35.545559
TE	1	1	30	39	1.8809	1.8876	35.545559
TE	1	1	31	40	1.885	1.8922	38.359711
TE	1	1	32	41	1.885	1.8922	38.359711
TE	1	1	33	42	1.8875	1.8951	40.012755
TE	1	1	34	43	1.8875	1.8951	40.012755
TE	1	1	35	44	1.8887	1.8965	41.355474
TE	1	1	36	45	1.8887	1.8965	41.355474

9-cell TESLA cavity, but can also be applied to a design with fewer cells. Fig. 9 demonstrates the tracking for a 3-cell TESLA cavity showing only the algebraic mapping for clarity, classifying the first 15 eigenmodes, corresponding to the first monopole and the first and second dipole passband. We observe analogous results to those of the 9-cell geometry. Each passband consists of the same number of eigenmodes as the cavity of cells, if disregarding the multiplicity of eigenmodes. In the first monopole passband, the lowest eigenmode is classified as TM010 and in the first dipole passband as TE111. The longitudinal index is accordingly increased.

D. Exploration of Eigenmodes

The described tracking algorithm can be used to directly calculate a specific eigenmode in the TESLA cavity without

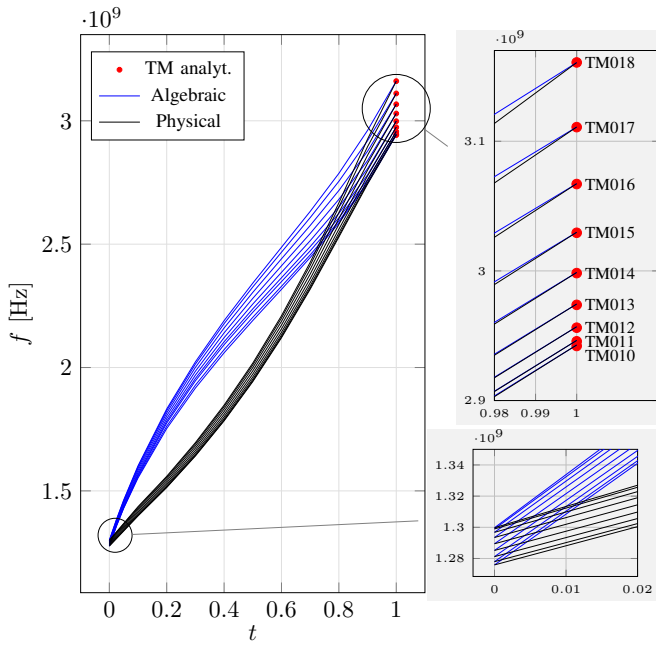


Fig. 7. Identification of the first monopole passband in the 9-cell TESLA cavity using algebraic and physical mappings from the TESLA cavity ($t = 0$) to pillbox ($t = 1$).

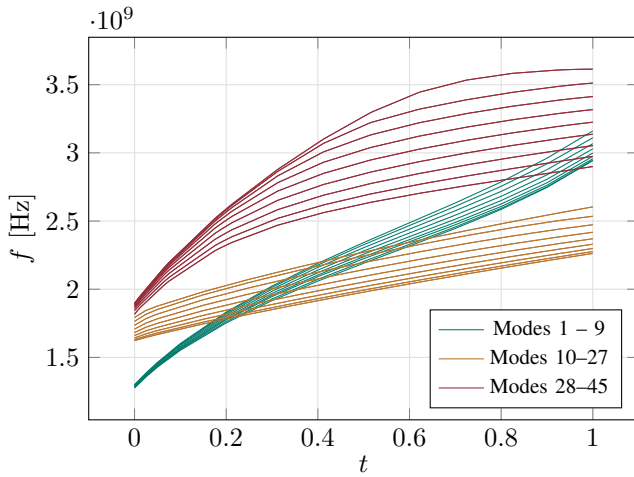


Fig. 8. Identification of eigenmodes $j = 1, \dots, 45$ of the 9-cell TESLA cavity applying the algebraic mapping from TESLA cavity ($t = 0$) to pillbox ($t = 1$).

the need to identify all eigenmodes. For this purpose, the eigenvalue $\lambda_{1,j}$ for chosen indices m , n and p is determined for the pillbox cavity and the corresponding eigenpair is tracked as described in Section IV-C. This is exemplified for eigenmode TM0117, which is the highest eigenmode in the second monopole passband for the 9-cell TESLA cavity in Fig. 10. Firstly, applying (1), the resonance frequency for the indices $m = 0$, $n = 1$ and $p = 17$ is computed at approx. 3.83 GHz. The eigenvalue problem (9) is solved for the pillbox cavity and the eigenmode with the closest eigenfrequency is tracked to approx. 2.44 GHz in the TESLA cavity. The tracking results are displayed in Fig. 10. The results

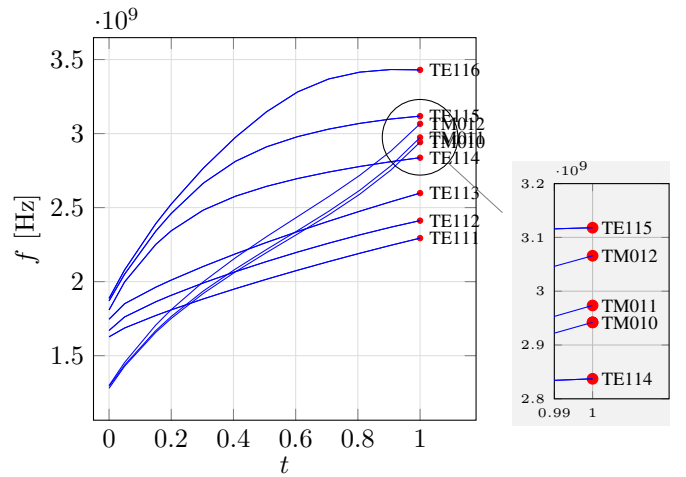


Fig. 9. Identification of the eigenmodes $j = 1, \dots, 15$ of the 3-cell TESLA cavity applying the algebraic mapping from TESLA cavity ($t = 0$) to pillbox ($t = 1$).

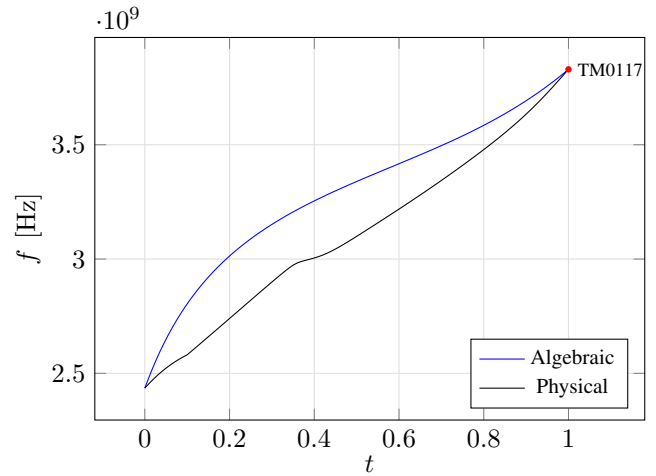


Fig. 10. Exploration of eigenmode TM0117 from the pillbox ($t = 1$) down to the 9-cell TESLA cavity ($t = 0$).

for the physical mapping are plotted and in Fig. 11, where the deformation of the magnitude of the magnetic field is illustrated.

E. Efficiency

If only one mode at a time is considered, then using Newton's method to solve the eigenvalue problem in each step, see e.g. [3] may be an efficient alternative to the Arnoldi method used above. However, this might be less robust since Newton's method may converge to a wrong mode. In particular, when the step size h_i is small, one may expect fast convergence of Newton's method due to availability of good initial guesses from the previous step, see (14). Let us consider an example in which we use the number of solved linear systems and the time for tracking the accelerating eigenmode for the 9-cell cavity as efficiency measure. We employ the algebraic mapping for a fixed stepsize of $h = 0.1$ such that no step size reduction is necessary. The computations are performed on a workstation with an Intel(R) CPU i7-3820 3.6 GHz processor and 13 GB

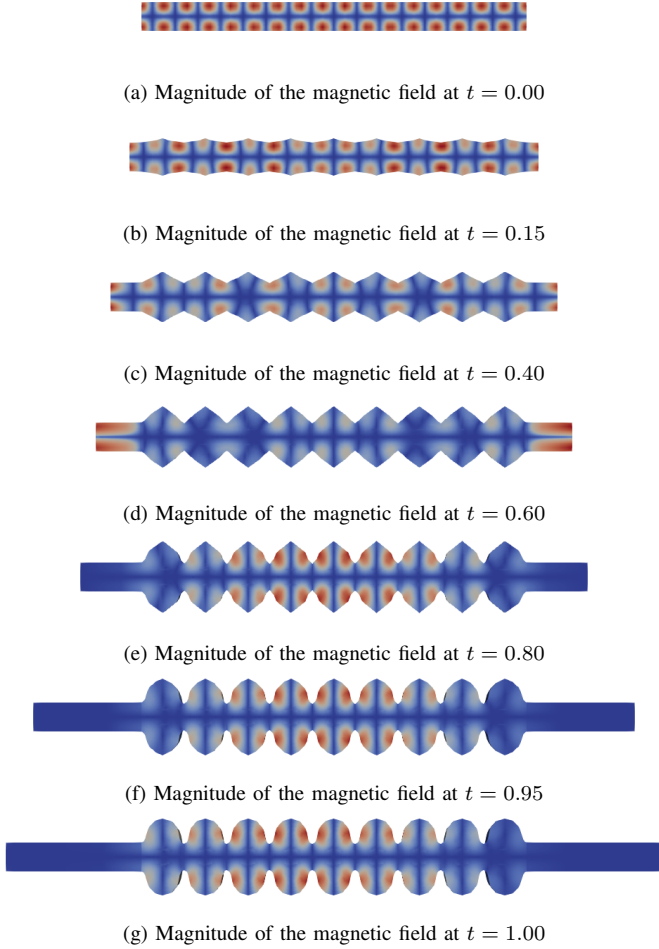


Fig. 11. Magnetic field magnitude of the eigenmode TM_{0117} (i.e. the highest eigenmode of the second monopole passband) along the physical deformation for exploration in the TESLA cavity.

RAM. The cost for assembly of the system matrices $\mathbf{K}(0)$, $\mathbf{M}(0)$, $\mathbf{K}(1)$ and $\mathbf{M}(1)$ is excluded. All time measurements are repeated 10 times and averaged. The eigenvalue problems are solved using Matlab's `eigs` which uses internally ARPACK [23], [27]. Classifying the accelerating eigenmode using the presented method requires 1571 systems of equations to be solved and on average 58.69s, while the tracking based on Newton's method solves 297 linear systems in 37.29s.

If $N_{\text{tracked}} > 1$ eigenmodes are of interest, then the efficiency of the tracking method in section IV-A can be increased by considering all of them at once. Since we always compute $N > N_{\text{tracked}}$ eigenpairs per step, this does not significantly increase the computational time of the eigenvalue solver, which is the most expensive component of the procedure. Yet, the complexity of the matching increases quadratically, or more precisely $N_{\text{tracked}} \cdot N$, since each mode of interest must be compared with all modes at the next step. Nevertheless, those costs remain negligible in comparison to the eigenvalue solver, even if hundreds of modes would be tracked.

VI. CONCLUSION AND OUTLOOK

In this work, we investigate an eigenmode tracking procedure and apply it for the automatic classification of eigenmodes in electromagnetic cavities. To this end, we employ shape morphing from complex geometries to the analytical pillbox cavity. By matching our numerical results with the analytic values, we are able to convey the well-known nomenclature based on the type of the eigenmodes (TE or TM) and the directional indices m , n and p and their intuition on more complex cavity shapes. By performing our algorithm in a backward manner, we can explore specific eigenmodes in a cavity.

We have shown that despite of eigenvalue crossings, our approach reliably tracks the eigenmodes also in 9-cell TESLA cavities, in contrast to field extrema counting methods, e.g. [14]. The numerical efficiency of our tracking method could be further improved by enhancing the prediction step (14) with higher order Taylor expansion [25] or by reducing our system matrices to a subspace of eigenpairs [32]. Furthermore, the accuracy of the derivatives of the system matrices can be improved by formulating them as shape derivatives along the geometry deformation [33].

REFERENCES

- [1] B. Aune, R. Bandelmann, D. Bloess, B. Bonin, A. Bosotti, M. Champion, C. Crawford, G. Deppe, B. Dwersteg, D. A. Edwards, H. T. Edwards, M. Ferrario, M. Fouaidy, P.-D. Gall, A. Gamp, A. Gössel, J. Graber, D. Hubert, M. Hüning, M. Juillard, T. Junquera, H. Kaiser, G. Kreps, M. Kuchnir, R. Lange, M. Leenen, M. Liepe, L. Lilje, A. Matheisen, W.-D. Möller, A. Mosnier, H. Padamsee, C. Pagani, M. Pekeler, H.-B. Peters, O. Peters, D. Proch, K. Rehlich, D. Reschke, H. Safa, T. Schilcher, P. Schmüser, J. Sekutowicz, S. Simrock, W. Singer, M. Tigner, D. Trines, K. Twarowski, G. Weichert, J. Weisend, J. Wojtkiewicz, S. Wolff, and K. Zapfe, "Superconducting TESLA cavities," *Phys. Rev. Accel. Beams*, vol. 3, no. 9, p. 092001, 2000.
- [2] V. Shemelin, H. Padamsee, and R. Geng, "Optimal cells for TESLA accelerating structure," *Nucl. Instrum. Meth. A*, vol. 496, no. 1, pp. 1–7, 2003.
- [3] N. Georg, W. Ackermann, J. Corno, and S. Schöps, "Uncertainty quantification for Maxwell's eigenproblem using isogeometric analysis and mode tracking," *Comput. Meth. Appl. Mech. Eng.*, vol. 350, pp. 228–244, Jun. 2019.
- [4] J. Corno, N. Georg, S. Gorgi Zadeh, J. Heller, V. Gubarev, T. Roggen, U. Römer, C. Schmidt, S. Schöps, J. Schultz, A. Sulimov, and U. van Rienen, "Uncertainty modeling and analysis of the european X-ray free electron laser cavities manufacturing process," *Nucl. Instrum. Meth. A*, vol. 971, p. 164135, May 2020.
- [5] K. Halbach and R. F. Holsinger, "SUPERFISH – a computer program for evaluation of RF cavities with cylindrical symmetry," *Particle Accelerators*, vol. 7, pp. 213–222, 1976.
- [6] U. van Rienen and T. Weiland, "Triangular discretization method for the evaluation of RF-fields in cylindrically symmetric cavities," *IEEE Trans. Magn.*, vol. 21, no. 6, pp. 2317–2320, Nov. 1985.
- [7] T. Weiland, "On the unique numerical solution of Maxwellian eigenvalue problems in three dimensions," *Particle Accelerators*, vol. 17, no. 227–242, 1985.
- [8] M. Ainsworth, J. Coyle, P. D. Ledger, and K. Morgan, "Computing Maxwell eigenvalues by using higher order edge elements in three dimensions," *IEEE Trans. Magn.*, vol. 39, no. 5, pp. 2149–2153, Sep. 2003.
- [9] S. Zaglmayr, "High order finite element methods for electromagnetic field computation," Dissertation, Johannes Kepler Universität, 2006.
- [10] J. A. Cottrell, T. J. R. Hughes, and Y. Bazilevs, *Isogeometric Analysis: Toward Integration of CAD and FEA*. Wiley, 2009.
- [11] J. Corno, C. de Falco, H. De Gerssem, and S. Schöps, "Isogeometric simulation of Lorentz detuning in superconducting accelerator cavities," *Comput. Phys. Comm.*, vol. 201, pp. 1–7, Feb. 2016.

- [12] W. Ackermann, H. De Gersem, C. Liu, and T. Weiland, "Eigenmode calculations for the TESLA cavity considering wave-propagation losses through fundamental and higher-order mode couplers," DESY, Internal Report PUBDB-2015-05269, 2015. [Online]. Available: <https://bib-pubdb1.desy.de/record/289143>
- [13] R. Wanzenberg, "Monopole, dipole and quadrupole passbands of the TESLA 9-cell cavity," DESY, Technical Report, 2001.
- [14] K. Brackebusch, T. Galek, and U. van Rienen, "Automated mode recognition algorithm for accelerating cavities," in *Proceedings of IPAC 2014, Dresden, Germany*, 2014, pp. 409–411.
- [15] J. D. Jackson, *Classical Electrodynamics*, 3rd ed. Wiley & Sons, 1998.
- [16] E. Cohen, R. F. Riesenfeld, and G. Elber, *Geometric Modeling with Splines: An Introduction*. CRC Press, 2001.
- [17] C. de Boor, *A Practical Guide to Splines*, rev. ed., ser. Applied Mathematical Sciences. Springer, 2001, vol. 27.
- [18] J. Corno, "Numerical methods for the estimation of the impact of geometric uncertainties on the performance of electromagnetic devices," Dissertation, Technische Universität Darmstadt, Jun. 2017.
- [19] P. Monk, *Finite Element Methods for Maxwell's Equations*. Oxford University Press, 2003.
- [20] D. Boffi, "Finite element approximation of eigenvalue problems," *Acta Num.*, vol. 19, pp. 1–120, May 2010.
- [21] A. Buffa, G. Sangalli, and R. Vázquez, "Isogeometric analysis in electromagnetics: B-splines approximation," *Comput. Meth. Appl. Mech. Eng.*, vol. 199, pp. 1143–1152, 2010.
- [22] R. Vázquez, "A new design for the implementation of isogeometric analysis in Octave and Matlab: GeoPDEs 3.0," *Comput. Math. Appl.*, vol. 72, no. 3, pp. 523–554, Aug. 2016.
- [23] Mathworks, *MATLAB Getting Started Guide*, 2020, 9.8.0 (R2020a).
- [24] S. H. Lui, H. B. Keller, and T. W. C. Kwok, "Homotopy method for the large, sparse, real nonsymmetric eigenvalue problem," *SIAM J. Matrix. Anal. Appl.*, vol. 18, no. 2, pp. 312–333, Apr. 1997.
- [25] P. Jorkowski and R. Schuhmann, "Mode tracking for parametrized eigenvalue problems in computational electromagnetics," in *2018 International Applied Computational Electromagnetics Society (ACES) Symposium*, B. M. Notaros, Ed. IEEE, Mar. 2018, p. 17803096.
- [26] E. Safin and D. Manteuffel, "Advanced Eigenvalue Tracking of Characteristic Modes," *IEEE Transactions on Antennas and Propagation*, vol. 64, no. 7, pp. 2628–2636, July 2016.
- [27] R. B. Lehoucq, D. C. Sorensen, and C. Yang, *Arpack User's Guide: Solution of Large-Scale Eigenvalue Problems With Implicitly Restarted Arnoldi Methods (Software, Environments, Tools)*. Society for Industrial and Applied Mathematics (SIAM), 1998.
- [28] I. U. Ojalvo, "Gradients for large structural models with repeated frequencies," in *Aerospace Technology Conference and Exposition*. SAE International, Oct. 1986, 861789.
- [29] R. L. Dailey, "Eigenvector derivatives with repeated eigenvalues," *AIAA J.*, vol. 27, no. 4, pp. 486–491, 1989.
- [30] D. Edwards, "TESLA test facility linac design report," DESY, Technical Report 95-01, Mar. 1995.
- [31] A. Ziegler, N. Georg, W. Ackermann, and S. Schöps, *Software for Mode Recognition by Shape Morphing for Maxwell's Eigenvalue Problem*, Jan. 2022. [Online]. Available: <https://github.com/amz78/Mode-Recognition>, doi: 10.5281/zenodo.6303315.
- [32] D. Yang and V. Ajjarapu, "Critical eigenvalues tracing for power system analysis via continuation of invariant subspaces and projected Arnoldi method," *IEEE Trans. Power Sys.*, vol. 22, no. 1, pp. 324–332, Feb. 2007.
- [33] K. Sturm, "On shape optimization with non-linear partial differential equations," Dissertation, Technische Universität Berlin, 2015.